

# Classical representation for quantum states of a particle in $\lambda z^{2m}$ potential

T.P. Grozdanov<sup>1</sup> and E.A. Solov'ev<sup>2</sup>

<sup>1</sup>Institute of Physics, University of Belgrade, Pregrevica 118, 11080 Belgrade, Serbia

Email: tasko@ipb.ac.rs

<sup>2</sup>Bogoliubov Laboratory for Theoretical Physics, Joint Institute for Nuclear Research,

Dubna, 141980 Moscow Region, Russia

Email: esolovev@theor.jnr.ru

## Abstract

A classical representation for quantum eigenstates of a particle bound in  $\lambda z^{2m}$  ( $\lambda > 0, m = 1, 2, \dots$ ) potentials is developed. It is represented by ensembles of classical trajectories with energy distributions that can take on negative values, for  $m > 1$  have integrable singularities at zero energy and whose mean energies coincide with quantum eigenenergies. The corresponding Schrödinger equation in classical representation is analyzed.

## 1 Introduction

Various aspects of relationship between classical and quantum mechanics are commonly explored by studying subjects such as: semiclassical quantization, limiting process  $\hbar \rightarrow 0$ , WKB approximation, measurement problem, quantum chaos, decoherence and alike (see, for example review [1]). An intriguing interplay between classical and quantum mechanics was introduced in the formulation of the *classical*

*representation* of quantum states in 1D [2]. Stationary quantum states are represented by ensembles of classical trajectories with energy distributions whose mean values are equal to quantum eigenenergies. However, being of non-classical origin these distributions can take negative values and therefore, similarly to Wigner functions, belong to class of quasiprobability distributions. Nevertheless we will refer to them in this work simply as to energy distributions. They are related to quantum position distributions via Abel transform and are solutions of the Schrödinger equation in classical representation. The latter takes form of an integrodifferential equation and can be interpreted as a balance equation with respect to some virtual exchange between classical states with energies  $\varepsilon$  and  $\tilde{\varepsilon}$  due to sub-barrier penetration [2]. This interpretation has a profound connection with the treatment of quantum physics as the theory of *the global information field* [3]. Some solvable problems have been considered in classical representation: harmonic oscillator, V-shaped potential  $\lambda |z|$ , time-dependent Feynman model for inelastic transitions in harmonic oscillator driven by time dependent external force [2, 4] and restricted model of s-states of hydrogen atom [5]. In addition, semiclassical approximation in classical representation was formulated [6].

In the present work we study the classical representation for oscillators with potentials  $\lambda z^{2m}$ . These potentials belong to wider family of polynomial potentials which have been widely used in various aspects of solving the corresponding 1D Schrödinger equation: perturbation expansions [7], high-order WKB solutions [8, 9, 10], high-precision numerical solutions [11, 12] and exact solutions [13, 14]. Additional motivation for studying these potentials is due to the fact that in the limit  $m \rightarrow +\infty$  they tend to a square well with infinite (impenetrable) walls. As mentioned above the concept of classical representation relies on peculiar treatment of quantum tunneling [2]. Tunneling is absent in the case of infinite square well and a direct construction of classical representation in that case is problematic. We shall explore if some clarification can be gathered by studying the evolution of the classical representations for  $\lambda z^{2m}$  potentials in the  $m \rightarrow +\infty$  process. We mention that similar problems occur in construction of classical representations for other systems without tunneling such

as 2D rigid rotor of treatment of azimuthal ( $\varphi$ -dependent) degree of freedom in 3D central potential problem.

The plan of the article is as follows. In Sect. 2 we present results of numerical calculations of quantum position distributions and eigenenergies of eigenstates. Section 3 introduces Abel transform which relates the quantum position distributions with classical energy distributions. In Sect. 4 we present and discuss numerically obtained energy distributions of classical ensembles corresponding to ground and excited states in various  $x^{2m}$  potentials. Section 5 contains the discussion of the form and peculiarities of the Schrödinger equation in classical representation for  $x^{2m}$  potentials. Our conclusions are given in Sect. 6.

## 2 Quantum position probability distributions

Schrödinger equation for stationary states  $\phi_n(z)$  ( $-\infty < z < +\infty, n = 0, 1, 2, \dots$ ) of a particle of mass  $\mu$  in potential  $\lambda z^{2m}$  ( $\lambda > 0, m = 1, 2, \dots$ ) is

$$\frac{d^2\phi_n(z)}{dz^2} + \frac{2\mu}{\hbar^2} [E_n - \lambda z^{2m}] \phi_n(z) = 0. \quad (1)$$

Introducing new independent variable  $x$  and new spectral parameter  $\varepsilon_n$ :

$$z = \beta x, \quad E_n = \gamma \varepsilon_n, \quad \beta = \left( \frac{\hbar^2}{2\mu\lambda} \right)^{\frac{1}{2m+2}}, \quad \gamma = \lambda \beta^{2m}, \quad (2)$$

(1) is transformed into

$$\frac{d^2\psi_n(x)}{dx^2} + [\varepsilon_n - x^{2m}] \psi_n(x) = 0. \quad (3)$$

Once we solve for normalized eigenfunctions  $\psi_n(x)$  and position probability distributions  $\rho_n(x) = \psi_n^2(x)$ , the normalized eigenfunctions  $\phi_n(z)$  and position probability distributions  $\tilde{\rho}_n(z) = \phi_n^2(z)$  are related to them by

$$\phi_n(z) = \frac{\psi_n(z/\beta)}{\sqrt{\beta}}, \quad \tilde{\rho}_n(z) = \frac{\rho_n(z/\beta)}{\beta}. \quad (4)$$

Therefore, in the rest of the paper we shall address only the eigenvalue problem (3). The case  $m = 1$  (harmonic oscillator) has well known solutions

$$\rho_n(x) = \frac{1}{\sqrt{\pi} 2^n n!} e^{-x^2} H_n^2(x), \quad \varepsilon_n = 2n + 1, \quad (5)$$

where  $H_n(x)$  are Hermite polynomials. The case  $m \rightarrow +\infty$  is also analytically solvable, because then the potential  $x^{2m}$  corresponds to square well with infinitely high walls located at  $x = -1$  and  $x = +1$ . The solutions are

$$\rho_n(x) = \sin^2[\pi(n+1)(x+1)/2], \quad \varepsilon_n = \frac{\pi^2}{4}(n+1)^2. \quad (6)$$

In all other cases the eigenvalue problem (3) has to be solved numerically.

In our calculations we have used a very efficient double exponential Sinc collocation method [12]. Figure 1 shows position probability distributions for the ground states ( $n = 0$ ) of various confining potentials  $x^{2m}$ . The black points define values of distributions at classical turning points  $x_{tp} = \varepsilon_0^{1/(2m)}$ . As  $m$  increases the distributions are "pushed" towards the region  $|x| < 1$  ending up with  $\rho_0(x)$  from (6).

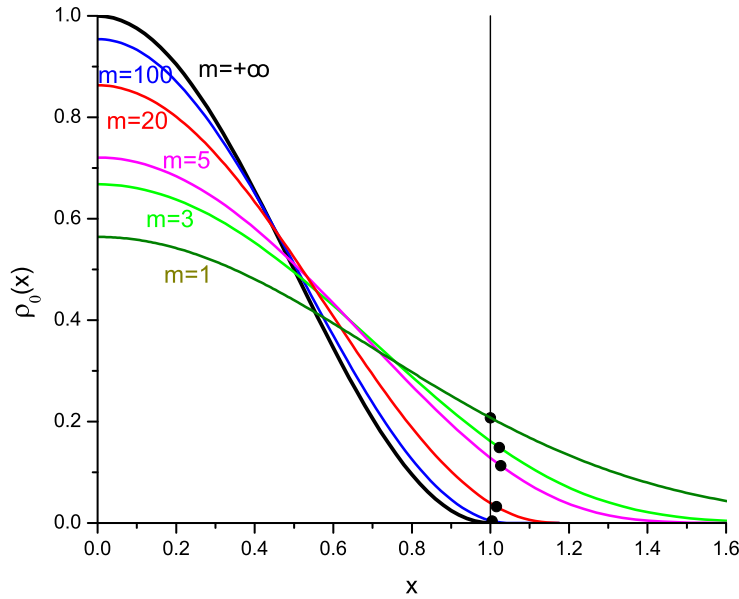


Figure 1: Ground-state position probability distributions  $\rho_0(x) = \rho_0(-x)$  in various confining potentials  $x^{2m}$ . The values of distributions at classical turning points are marked by black points. Vertical thin line indicates the position of the infinite wall of the limiting ( $m \rightarrow +\infty$ ) square well potential.

In Fig. 2 the curve labeled "exact" shows ground-state eigenvalues  $\varepsilon_0$  for various

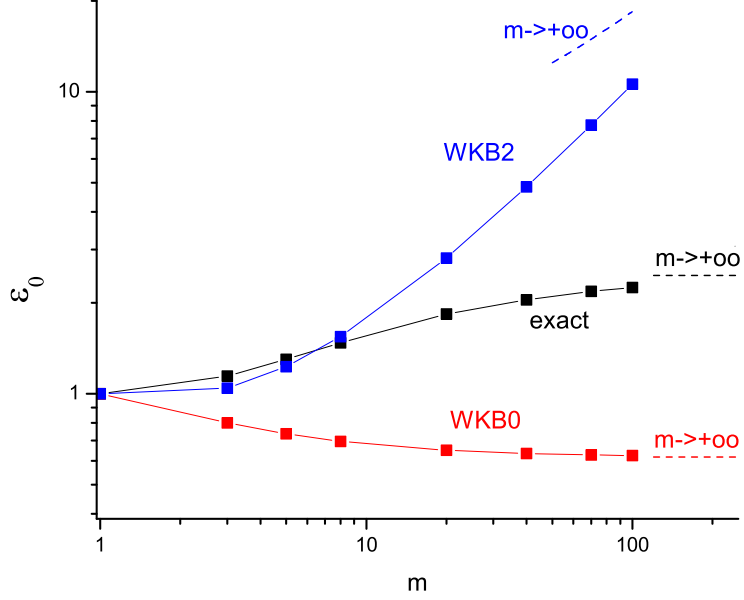


Figure 2: Ground state eigenvalues  $\varepsilon_0$  for various confining potentials  $x^{2m}$ . Numerical results are represented by black symbols (curve labeled exact). Zeroth and second order WKB approximations (curves labeled WKB0 and WKB2) are represented by red and blue symbols. Asymptotes corresponding to  $m \rightarrow \infty$  are represented by dashed lines.

values of  $m$ . The asymptotic approach to  $m = +\infty$  value  $\varepsilon_0 = \pi^2/8$  from (6) (the thin horizontal black dashed line) is indicated.

For the sake of illustrative comparison we have also calculated eigenvalues using the WKB approximation. Explicit expressions for the ordinary (zeroth order)  $\varepsilon_n^0$  and the second order  $\varepsilon_n^2$  (which includes the correction of order  $\hbar^2$ ) WKB approximations have been derived in [8]:

$$(\varepsilon_n^0)^{\frac{m+1}{2m}} = \frac{\pi m}{B_1} (n + 1/2), \quad (7)$$

$$(\varepsilon_n^2)^{\frac{m+1}{2m}} = \frac{\pi m}{2B_1} \left[ n + 1/2 + \left( (n + 1/2)^2 + \frac{B_1 B_2 (2m-1)(m-1)}{6\pi^2 m^2} \right)^{1/2} \right], \quad (8)$$

$$B_1 = B \left( \frac{1}{2m}, \frac{3}{2} \right), \quad B_2 = B \left( 1 - \frac{1}{2m}, \frac{1}{2} \right) \quad (9)$$

and  $B(p, q) = \Gamma(p)\Gamma(q)/\Gamma(p+q)$  is the beta function. In the case of harmonic oscillator

( $m=1$ ) we find  $\varepsilon_n^0 = \varepsilon_n^2 = \varepsilon_n = 2n + 1$ . If we let  $m \rightarrow +\infty$  in (7) and (8) we find

$$\varepsilon_n^0 \rightarrow \frac{\pi^2}{4}(n + 1/2)^2, \quad (10)$$

$$\varepsilon_n^2 \rightarrow \frac{\pi^2}{16} \left\{ n + 1/2 + \left[ (n + 1/2)^2 + \frac{4m}{3\pi^2} \right]^{1/2} \right\}^2, \quad (11)$$

so that  $\varepsilon_n^0$  tends to constant value (10) (which for large  $n$  is consistent with (6)) while  $\varepsilon_n^2$  diverges for large  $m$ .

For the ground state, as seen from Fig.2 the  $\varepsilon_0^0$  (curve labeled WKB0) as expected performs bad. On the other hand, the  $\varepsilon_0^2$  (curve labeled WKB2) provides reasonable predictions until  $m \approx 8$  when it deviates toward the asymptote (11) which is shown as dashed blue curve.

As a representative of excited states we shall take the  $n = 4$  state. Figure 3 shows quantum position densities for  $n = 4$  states for various  $x^{2m}$  potentials. With the increase of  $m$  distributions are pushed towards the region  $-1 < x < 1$  approaching asymptotically the distribution (6) of the particle in the box with infinite walls.

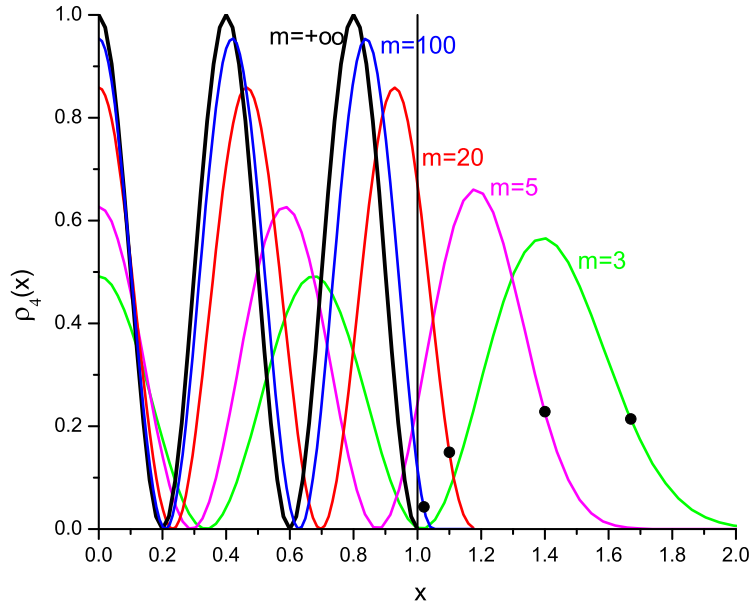


Figure 3: Same as Fig.1 but for excited  $n = 4$  state.

The eigenvalues  $\varepsilon_4$  as a function of  $m$  are shown in Figure 4 as black points and the corresponding asymptotic value (6) as dashed black line. The zeroth order WKB approximation  $\varepsilon_4^0$  (curve labeled WKB0) performs much better than in the case of ground state, but somewhere around  $m = 8$  departs from the vicinity of the exact results and eventually approach its asymptote (10) (red dashed line). The second order approximation  $\varepsilon_4^2$  (curve labeled WKB2) performs even better and for larger  $m$  but also departs from the vicinity of the exact values around  $m = 40$  and approach its asymptote (11) (dashed blue curve) .

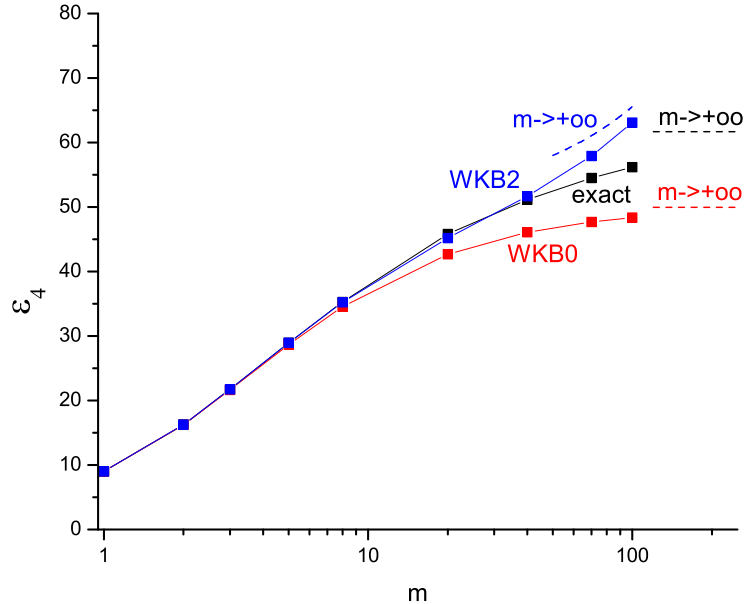


Figure 4: Same as Fig2 but for  $n = 4$  states.

The zeroth and second order WKB approximations have been used here for illustrative purposes. It should be mentioned that elaborate techniques exist for calculating very high order WKB approximations related to  $x^{2m}$  potentials, which are very accurate, especially for excited states [9, 10].

### 3 Classical representation and Abel transform

For the class of symmetric potentials  $V(-x) = V(x)$ ,  $V(0) = 0$  that monotonically increase for  $x > 0$  the detailed procedure for construction of classical representation was developed in [2]. Since the potential  $v(x) = x^{2m}$  belongs to this class we closely follow that procedure.

An eigenstate with position distribution  $\rho_n(x)$  is represented as an ensemble of classical trajectories oscillating between the turning points  $-x_{tp}(\varepsilon)$  and  $x_{tp}(\varepsilon) = \varepsilon^{1/(2m)}$  and distributed over the energies  $\varepsilon$  in classically allowed region  $\varepsilon > v(x) = x^{2m}$  with a certain distribution  $f_n(\varepsilon)$ :

$$\rho_n(x) = \int_{x^{2m}}^{+\infty} q(\varepsilon, x) f_n(\varepsilon) d\varepsilon, \quad (12)$$

where the  $x$ -probability distribution for the classical ensemble  $q(\varepsilon, x)$  at energy  $\varepsilon$  is proportional to the time spent by particle in the interval  $dx$ :

$$q(\varepsilon, x) = \frac{2}{T(\varepsilon)} \frac{dt}{dx} = \frac{1}{T(\varepsilon) \sqrt{\varepsilon - x^{2m}}}, \quad (13)$$

and  $T(\varepsilon)$  is classical period

$$T(\varepsilon) = \int_{-\varepsilon^{1/2m}}^{\varepsilon^{1/2m}} \frac{dx}{\sqrt{\varepsilon - x^{2m}}} = \frac{1}{m} B \left( \frac{1}{2m}, \frac{1}{2} \right) \varepsilon^{\frac{1-m}{2m}}, \quad (14)$$

so that normalization condition holds

$$\int_{-\varepsilon^{1/2m}}^{\varepsilon^{1/2m}} q(\varepsilon, x) dx = 1. \quad (15)$$

The classical relations (13) and (14) hold because the classical hamiltonian related to Schrödinger equation (1) is

$$H_z^{cl} = \frac{p_z^2}{2\mu} + \lambda z^{2m}, \quad (16)$$

and after applying the change of variables (2) the classical hamiltonian related to Schrödinger equation (3) is

$$H_x^{cl} = p_x^2 + x^{2m}, \quad p_x = p_z / \sqrt{2\mu\gamma}, \quad (17)$$

so that the equation of motion is

$$\frac{dx}{dt} = \frac{\partial H_x^{cl}}{\partial p_x} = 2p_x = 2\sqrt{\varepsilon - x^{2m}}. \quad (18)$$

Due to the condition (15) the integration of (12) over  $x$  leads to the normalization condition of the distribution  $f_n(\varepsilon)$ :

$$\int_0^{+\infty} f_n(\varepsilon) d\varepsilon = \int_{-\infty}^{+\infty} \rho_n(x) dx = 1. \quad (19)$$

We can rewrite (12) as

$$\rho_n(x) = \int_v^{+\infty} \frac{f_n(\varepsilon)/T(\varepsilon)}{\sqrt{\varepsilon - v}} d\varepsilon. \quad (20)$$

It is the well known Abel transform with respect to variable  $v$ . Its reverse expression reads [15]

$$f_n(\varepsilon) = -\frac{T(\varepsilon)}{\pi} \int_{\varepsilon}^{+\infty} \frac{d\rho_n(x(v))}{dv} \frac{dv}{\sqrt{v - \varepsilon}}, \quad (21)$$

where  $x(v) = v^{\frac{1}{2m}}$  is the inverse function to  $v(x) = x^{2m}$ .

The transforms (20), (21) can be understood, in some broader sense, as connecting two representations of the same state [2]. The representation defined by  $f_n(\varepsilon)$  was called "classical representation" since the kernel  $q(\varepsilon, x)$  is the classical probability density and  $f_n(\varepsilon)$  has the meaning of the energy distribution in the classical ensemble. These distributions, as we shall see, can take negative values and therefore are quasiprobability distributions.

In addition, an important relation holds [2]

$$\int_0^{+\infty} \varepsilon f_n(\varepsilon) d\varepsilon = \varepsilon_n, \quad (22)$$

meaning that average energy of classical ensemble is equal to eigenenergy of quantum state .

## 4 Energy distributions $f_n(\varepsilon)$

In the case of harmonic oscillator ( $m = 1$ )  $f_n(\varepsilon)$  distributions are known analytically [2](see also section 5 below)

$$f_n(\varepsilon) = (-1)^n e^{-\varepsilon} L_n(2\varepsilon), \quad (23)$$

where  $L_n(x)$  is Laguerre polynomial.

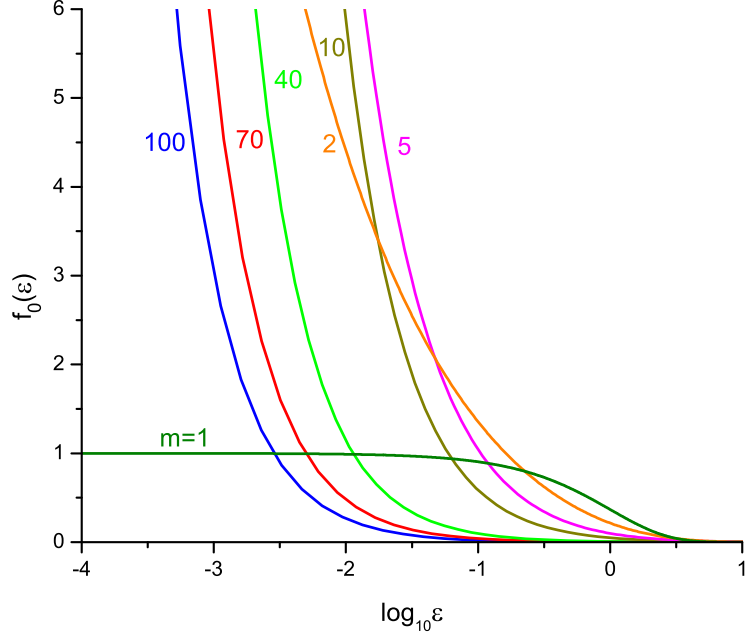


Figure 5: Ground-state energy distributions  $f_0(\varepsilon)$  for various  $x^{2m}$  potentials.

We used numerically calculated quantum distributions  $\rho_n(x)$  and numerical differentiation and integration in (21) to determine  $f_n(\varepsilon)$  for various quantum states and  $x^{2m}$  potentials. Figure 5 shows ground-state distributions  $f_0(\varepsilon)$  for a number of potentials with  $m = 1$  to  $m = 100$ . We see that in the limit  $\varepsilon \rightarrow 0$  only in the case of harmonic oscillator ( $m = 1$ )  $f_0(\varepsilon)$  remains finite (in accord with (23),  $f_0(0) = 1$ ) while in all other cases they diverge to  $+\infty$ . Closer inspection of the integral (21) for  $\varepsilon \rightarrow 0$  shows that the behavior of  $f_n(\varepsilon)$  distributions is given by (see Appendix)

$$\begin{aligned}
 f_n(0) &= (-1)^n & m = 1, \\
 f_n(\varepsilon) &\approx \frac{(-1)^n}{2\pi} |c_{n1}| B\left(\frac{1}{4}, \frac{1}{2}\right) \log(\varepsilon^{-\frac{1}{4}}) \varepsilon^{-\frac{1}{4}} & m = 2, \\
 f_n(\varepsilon) &\approx \frac{(-1)^n}{m\pi} |c_{n1}| B\left(\frac{1}{2m}, \frac{1}{2}\right) S_{m1} \varepsilon^{-1+\frac{3}{2m}} & m > 2, \\
 c_{n1} &= \frac{d^2 \rho_n(x)}{dx^2} |_{x=0}, \\
 S_{m1} &= \sum_{k=0}^{\infty} \frac{(2k-1)!!}{(2k)!![(2k+1)m-2]}.
 \end{aligned} \tag{24}$$

Note that indeed in Fig. 5 the slope of rising of  $f_0(\varepsilon)$  for the quartic potential ( $m = 2$ ) is different from other cases. The singularities (24) are integrable so that

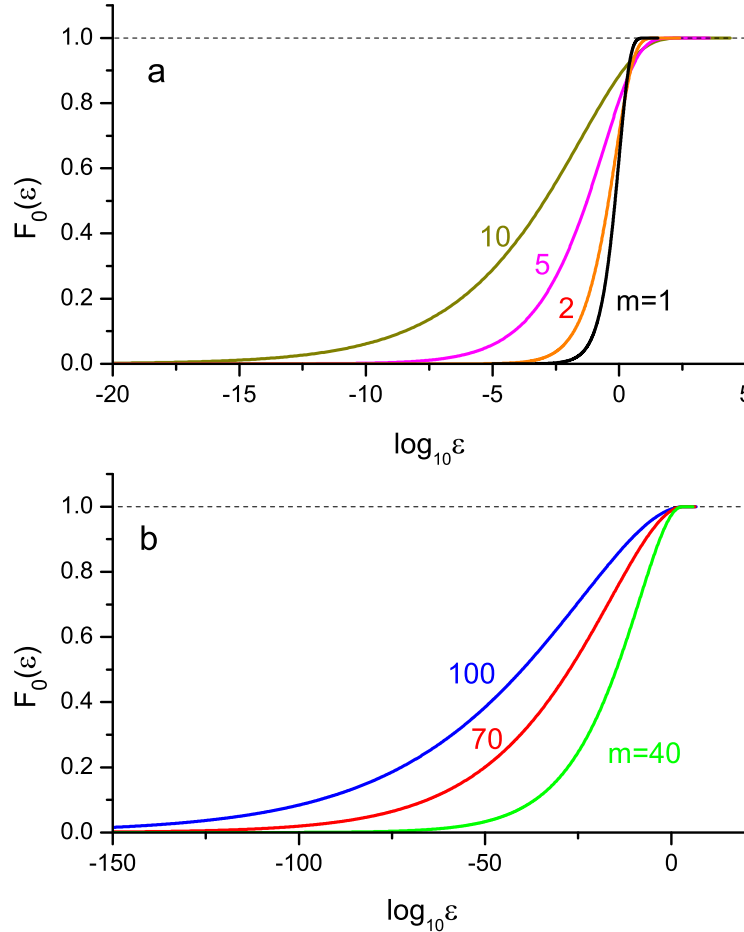


Figure 6: Ground-state cumulative energy distributions  $F_0(\varepsilon)$  for various  $x^{2m}$  potentials.

*cumulative* energy distributions are well defined:

$$F_n(\varepsilon) = \int_0^\varepsilon f_n(\tilde{\varepsilon}) d\tilde{\varepsilon}. \quad (25)$$

However, in the limit  $m \rightarrow +\infty$  the singularity is of the type  $\varepsilon^{-1}$ , that is nonintegrable, so that the existence of classical representation for the infinite square well is problematic.

Cumulative distributions corresponding to cases shown in Fig. 5 are shown in Fig. 6. We can see that as  $m$  increases the values of  $\varepsilon$  where  $F_0(\varepsilon)$  distributions are non negligible are getting closer to  $\varepsilon = 0$ . Results shown in Fig. 6 confirm the

normalization condition (19). In addition, we have verified by numerical integration that condition (22) is fulfilled in all cases.

Note that  $f_0(\varepsilon) > 0$  and  $F_0(\varepsilon) > 0$  for all values of  $m$  and therefore they are not quasiprobability distributions but rather ordinary probability distributions. Apparently, this occurs because the ground-state quantum position distributions  $\rho_0(x)$  are nodeless. This will not be the case with excited states.

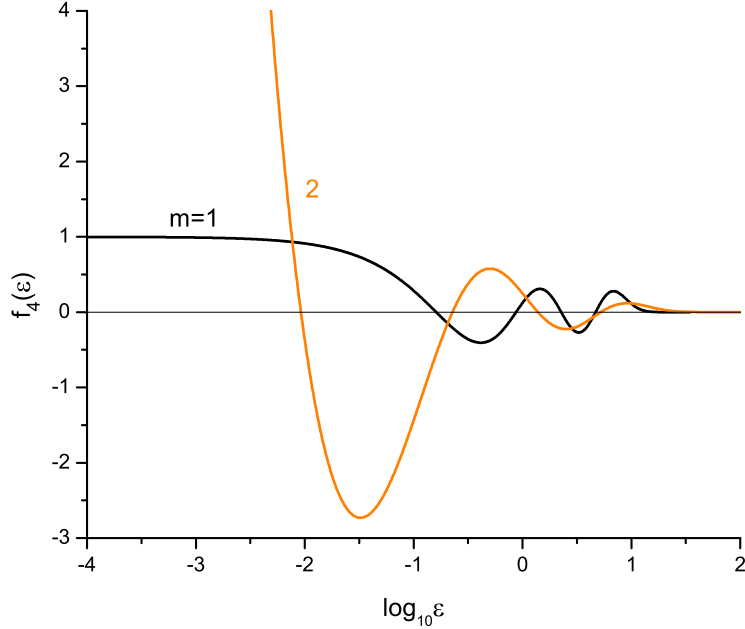


Figure 7: Excited-state ( $n = 4$ ) energy distributions  $f_4(\varepsilon)$  for harmonic ( $m = 1$ ) and quartic ( $m = 2$ ) oscillators.

In Fig. 7 we present results for  $n = 4$  excited states of harmonic ( $m = 1$ ) and quartic ( $m = 2$ ) oscillators, confirming the behavior of  $f_4(\varepsilon)$  distributions as predicted by (24). As  $m$  increases the amplitudes of oscillations of  $f_4(\varepsilon)$  enormously increase so that it is not possible to represent all details on a single figure. Figure 8 shows four different scales which are necessary to resolve all four nodes of  $f_4(\varepsilon)$  distribution in the  $m = 5$  case. Cumulative energy distributions are better adopted for compact presentation. Figure 9a shows  $F_4(\varepsilon)$  distributions corresponding to lower values of  $m$  and Fig. 9b those corresponding to higher values of  $m$ . In the cases of extremely high

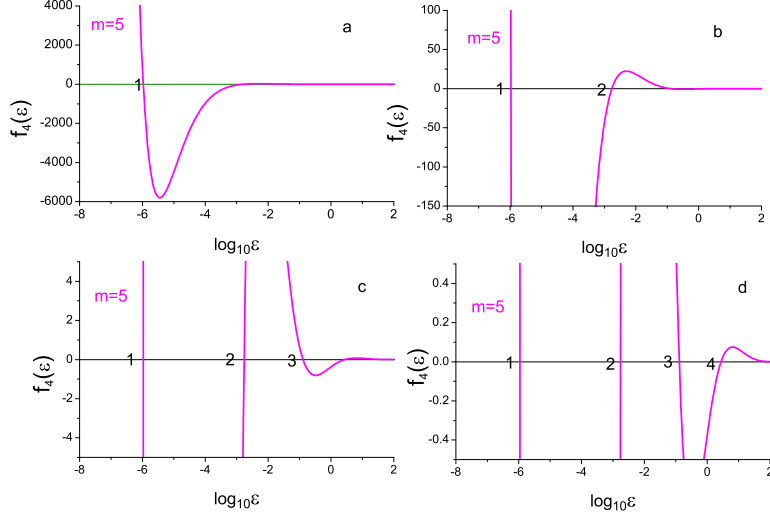


Figure 8: Same as Fig. 7 but for  $m = 5$  case and on four different scales of  $f_4(\varepsilon)$ . Points labeled with 1-4 are nodes of the  $f_4(\varepsilon)$  distribution.

values of  $m$  the regions where the  $F_4(\varepsilon)$  distributions are not negligible are extremely close to  $\varepsilon = 0$ . With the increase of  $m$  the nodes of distributions move toward  $\varepsilon = 0$ . These results also confirm the normalization condition (19) and we have verified by numerical integration that relation (22) holds in all cases.

We have chosen as examples two symmetric states ( $n = 0$  and  $n = 4$ ) and studied them for various values of  $m$ . In the case of antisymmetric states (odd  $n$ ) all properties of  $f_n(\varepsilon)$  and  $F_n(\varepsilon)$  distributions remain the same with the only difference that, according to (24), for  $m > 1$  the  $f_n(\varepsilon)$  distributions diverge to  $-\infty$  when  $\varepsilon \rightarrow 0$ .

The energy distributions  $\tilde{f}_n(E)$  and  $\tilde{F}_n(E)$  corresponding to  $V(z) = \lambda z^{2m}$  potential are related to  $f_n(\varepsilon)$  and  $F_n(\varepsilon)$  distributions through the simple relations

$$\tilde{f}_n(E) = f_n(E/\gamma)/\gamma, \quad \tilde{F}_n(E) = F_n(E/\gamma). \quad (26)$$

Considering the behavior of energy distributions  $f_n(\varepsilon)$  in the limit of  $m \rightarrow +\infty$ , some additional information can be obtained with an appropriate scaling of both  $f_n(\varepsilon)$  and  $\varepsilon$ . This is shown in Fig. 10 where the scaled distributions  $\text{sgn}f_4(\varepsilon) |f_4(\varepsilon)|^{\frac{1}{2m}}$  (with  $\text{sgn}f \equiv f/|f|$ ) as functions of  $\varepsilon^{\frac{1}{2m}}$  are shown for the cases  $m = 5$  and  $m = 100$ .

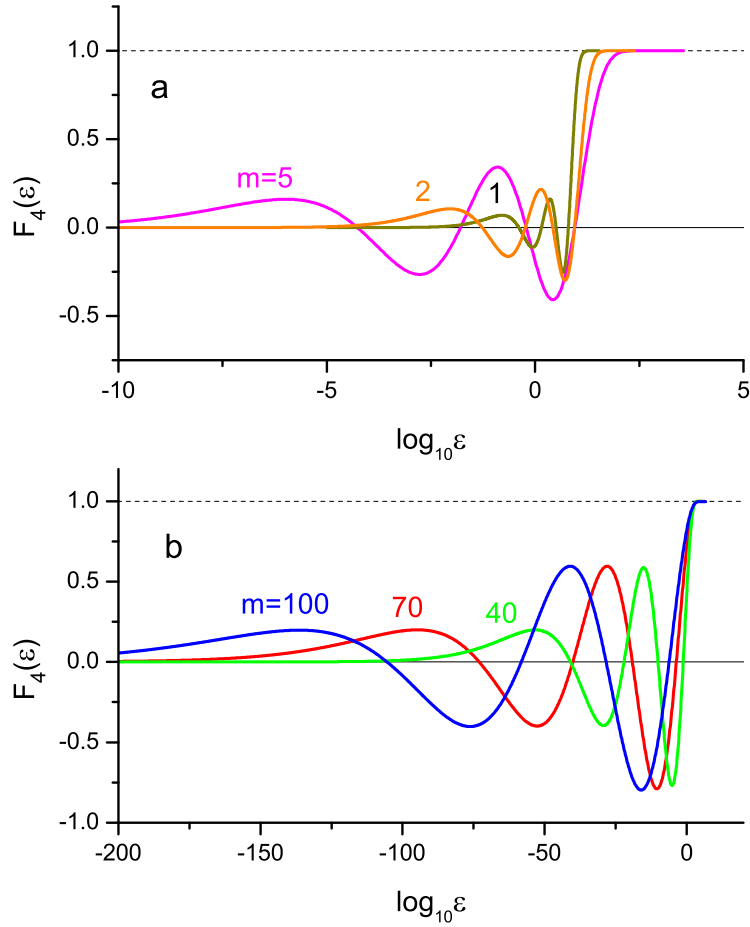


Figure 9: Excited-state ( $n = 4$ ) cumulative energy distributions  $F_4(\varepsilon)$  for various  $x^{2m}$  potentials.

Note that in the  $m = 5$  case the complete behavior of the scaled distribution is shown on the single graph, while for the unscaled quantities we needed four graphs, as seen from Fig. 8.

The result for the  $m = 100$  case in Fig. 10 suggests the following limiting form for the scaled energy distribution  $\text{sgn} f_n(\varepsilon) |f_n(\varepsilon)|^{\frac{1}{2m}}$  when  $m \rightarrow +\infty$ : For  $\varepsilon^{\frac{1}{2m}} < 1$ , it consists of alternating arcs which lie on  $\varepsilon^{-\frac{1}{2m}}$  and  $-\varepsilon^{-\frac{1}{2m}}$  curves with jumps at the nodes of the distribution defined by the expression

$$\varepsilon_k^{\frac{1}{2m}} = \frac{k}{n+1}, \quad k = 1, 2, \dots, n. \quad (27)$$

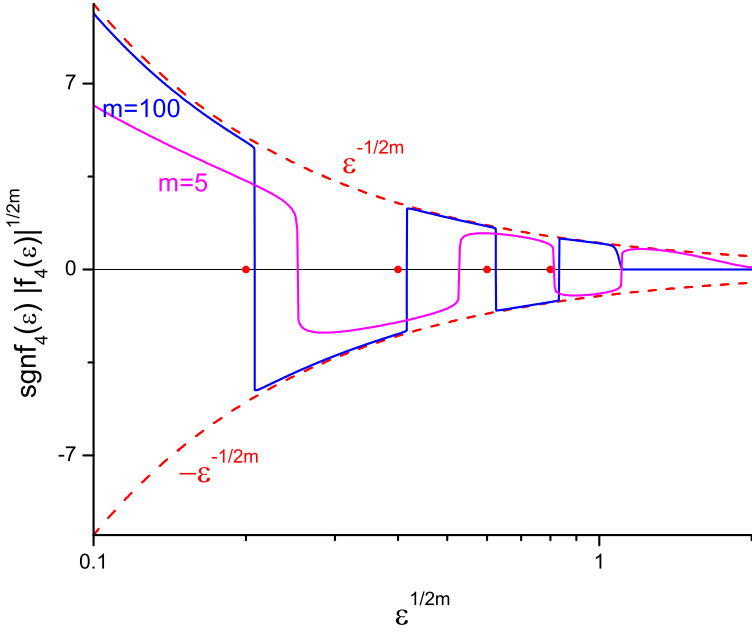


Figure 10: Scaled energy distributions  $\text{sgn}f_4(\varepsilon) |f_4(\varepsilon)|^{\frac{1}{2m}}$  as functions of  $\varepsilon^{\frac{1}{2m}}$  for the cases  $m = 5$  and  $m = 100$ . The red points are nodes (27) of the limiting distribution for  $m \rightarrow +\infty$ .

For  $\varepsilon^{\frac{1}{2m}} \approx 1$  there is abrupt fall of the distribution to zero. We have verified that this pattern is correct for other values of  $n$ . However, the emerging forms of distributions  $f_n(\varepsilon)$  all diverge as  $\pm 1/\varepsilon$  as  $\varepsilon \rightarrow 0$ , in accord with (24) and are therefore nonintegrable. Thus, the energy distributions for the infinite square well are not well defined, although for any potential  $x^{2m}$  with large but finite  $m$  they are well defined.

Thus the eigenstates of rectangular well in classical representation are new class of generalized functions which are located at the point  $\varepsilon = 0$  and have complicate structure providing orthonormalization conditions. For ground state, which satisfies normalization condition

$$\int_0^1 f_0^{\text{app.}}(\varepsilon) d\varepsilon = 1, \quad (28)$$

it is one of the possible representation of delta function  $\delta(x)$ .

Figure 10 provokes the wrong impression that the distribution  $f_n(\varepsilon)$  is negligible for  $\varepsilon > 1$ . In fact, it depends on what it is used for. For large  $m$ , there is a tail of the

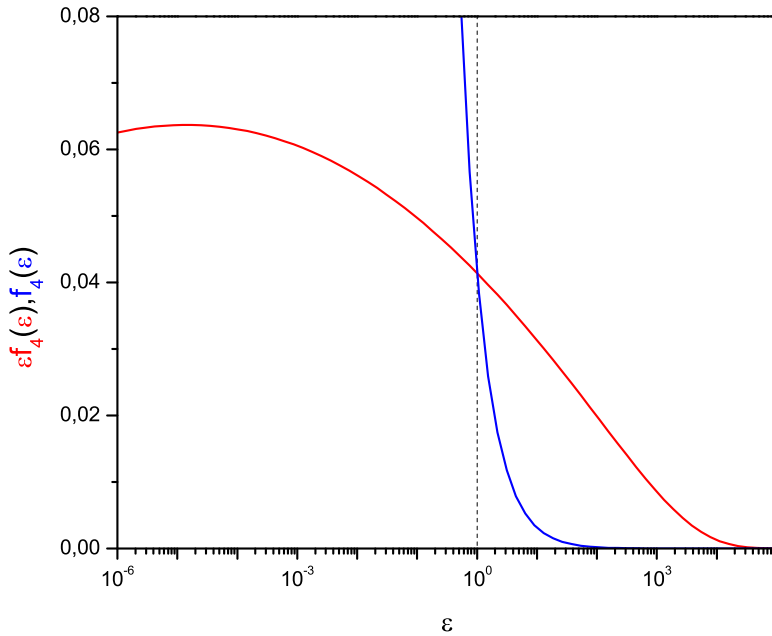


Figure 11: Distribution  $f_4(\varepsilon)$  (blue curve) and  $\varepsilon f_4(\varepsilon)$  (red curve) for  $m = 100$  as functions of  $\varepsilon$  in logarithmic scale.

distribution in the region  $\varepsilon > 1$ , which, for example, gives a dominant contribution to the calculation of the mean value of  $\varepsilon$ , which should coincide with the eigenvalue  $E_n$ . In Fig.11  $f_4(\varepsilon)$  and  $\varepsilon f_4(\varepsilon)$  are shown for  $n = 4$  and  $m = 100$  in a logarithmic scale, and the mean value

$$\bar{\varepsilon} = \int_0^\infty \varepsilon f_4(\varepsilon) d\varepsilon$$

coincides with the eigenenergy  $E_4 = 56.17$ . As can be seen from Fig.11, the region  $\varepsilon \leq 1$  contributes to  $\bar{\varepsilon}$  less than 0.06 (or 0.1% ).

## 5 Schrödinger equation in classical representation

It was shown in [2] that starting from the Schrödinger equation, in our case (3), one can derive the linear third-order differential equation for the position probability density  $\rho(x) = \psi(x)^2$

$$\frac{d^3\rho_n(x)}{dx^3} - 4[v(x) - \varepsilon_n] \frac{d\rho_n(x)}{dx} - 2 \frac{dv(x)}{dx} \rho_n(x) = 0, \quad (29)$$

where  $v(x) = x^{2m}$ . Introducing function

$$\varphi_n(\varepsilon) = \frac{f_n(\varepsilon)}{T(\varepsilon)} \quad (30)$$

and substituting (20) in (29) one arrives at integrodifferential equation [2]

$$(\varepsilon - \varepsilon_n)\varphi_n(\varepsilon) = \frac{2}{15\pi} \int_{\varepsilon^{\frac{1}{2m}}}^{+\infty} Q(\tilde{\varepsilon}, \varepsilon) \frac{d^3\varphi_n(\tilde{\varepsilon})}{d\tilde{\varepsilon}^3} d\tilde{\varepsilon} \quad (31)$$

with the kernel

$$Q(\tilde{\varepsilon}, \varepsilon) = \int_{\varepsilon^{\frac{1}{2m}}}^{\tilde{\varepsilon}^{\frac{1}{2m}}} (x^{2m} - \varepsilon)^{-1/2} \frac{d^3}{dx^3} (\tilde{\varepsilon} - x^{2m})^{5/2} dx. \quad (32)$$

The boundary conditions associated with eigenvalue problem (31) are for  $\varepsilon \rightarrow +\infty$

$$\varphi_n(\varepsilon) \rightarrow 0 \quad (33)$$

and for  $\varepsilon \rightarrow 0$  (see Appendix)

$$\begin{aligned} \varphi_n(0) &= \frac{(-1)^n}{\pi}, & m = 1, \\ \varphi_n(\varepsilon) &\approx \frac{(-1)^n}{\pi} |c_{n1}| \log(\varepsilon^{-\frac{1}{4}}), & m = 2, \\ \varphi_n(\varepsilon) &\approx \frac{(-1)^n}{\pi} |c_{n1}| S_{m1} \varepsilon^{-\frac{1}{2} + \frac{1}{m}}, & m > 2, \\ c_{n1} &= \frac{d^2\rho_n(x)}{dx^2} |_{x=0}, \\ S_{m1} &= \sum_{k=0}^{\infty} \frac{(2k-1)!!}{(2k)!![(2k+1)m-2]}, \end{aligned} \quad (34)$$

which is in accord with (14), (24) and (30).

Performing the integration in (32) one finds

$$Q(\tilde{\varepsilon}, \varepsilon) = \sum_{k=1}^3 c_k(m) I_k, \quad (35)$$

$$c_1(m) = -\frac{15m^2}{2}, \quad c_2(m) = \frac{45m(2m-1)}{2}, \quad c_3(m) = -5(2m-1)(m-1), \quad (36)$$

$$\begin{aligned} I_k &= \int_{\varepsilon}^{\tilde{\varepsilon}} (v - \varepsilon)^{-\frac{1}{2}} (\tilde{\varepsilon} - v)^{-\frac{3}{2}+k} v^{3-k-\frac{1}{m}} dv \\ &= \varepsilon^{3-k-\frac{1}{m}} (\tilde{\varepsilon} - \varepsilon)^{k-1} B\left(k - \frac{1}{2}, \frac{1}{2}\right) F\left(k - 3 + \frac{1}{m}, \frac{1}{2}; k; -\frac{\tilde{\varepsilon} - \varepsilon}{\varepsilon}\right) \end{aligned} \quad (37)$$

where  $F(a, b; c; z)$  is hypergeometric function and the integral was taken from [16].

Obviously, solving numerically integral equation (31) with the kernel (35) would be a challenging task. The direct solution of Abel transform (21) which we demonstrated in the previous section seems to be more efficient method.

One exception is the case ( $m=1$ ) of harmonic oscillator. In that case only the first two terms in (35) survive, the corresponding two hypergeometric functions in (37) reduce to polynomials and we find

$$Q(\tilde{\varepsilon}, \varepsilon) = \frac{15\pi}{2}(\tilde{\varepsilon} - 2\varepsilon). \quad (38)$$

Substituting (38) in (31) after partial integration the following differential equation is obtained

$$(\varepsilon - \varepsilon_n)\varphi_n(\varepsilon) = \varepsilon \frac{d^2\varphi_n(\varepsilon)}{d\varepsilon^2} + \frac{d\varphi_n(\varepsilon)}{d\varepsilon}. \quad (39)$$

Its solution obeying the boundary conditions (33) and (34) is

$$\varphi_n(\varepsilon) = \frac{(-1)^n}{\pi} e^{-\varepsilon} L_n(2\varepsilon), \quad \varepsilon_n = 2n + 1, \quad (40)$$

which is in accord with (30) and (23) since  $T(\varepsilon) = \pi$  for  $m = 1$ .

In terms of the non-scaled variables, that is for potential  $V(z) = \frac{1}{2}\mu\omega^2 z^2$ , we find from (2)  $\gamma = \hbar\omega/2$  and therefore

$$\tilde{f}_n(E) = \frac{f_n(\frac{E}{\gamma})}{\gamma} = (-1)^n \frac{2}{\hbar\omega} e^{-\frac{2E}{\hbar\omega}} L_n\left(\frac{4E}{\hbar\omega}\right), \quad E_n = \gamma\varepsilon_n = \hbar\omega(n + \frac{1}{2}), \quad (41)$$

which is the result found in [2] except for missing the factor  $(-1)^n$ .

Interestingly, in the limit  $m \rightarrow +\infty$ , the hypergeometric functions in (37) also reduce to polynomials and we find

$$Q(\tilde{\varepsilon}, \varepsilon) = -\frac{15\pi m^2}{16}(\tilde{\varepsilon}^2 - 18\tilde{\varepsilon}\varepsilon + 25\varepsilon^2), \quad (42)$$

which tends to infinity, confirming our earlier statement that the existence of classical representation for infinite square well is problematic.

## 6 Concluding remarks

We have presented a systematic study of classical representations for variety of potentials  $\lambda z^{2m}$ . The energy distributions  $f_n(\varepsilon)$  were determined by direct numerical solution of the Abel integral equation (21). It was found that, except for the  $m = 1$  case of harmonic oscillator, in all other cases the energy distributions diverge at  $\varepsilon = 0$ . These singularities are however integrable and cumulative energy distributions are well defined. We have also numerically verified that the mean energies of  $f_n(\varepsilon)$  distributions coincide with quantum eigenenergies  $\varepsilon_n$ . Although quantum position densities and eigenvalues for  $m \rightarrow +\infty$  tend towards those of the infinite square well potential, this limit in the case of  $f_n(\varepsilon)$  distributions lead to nonintegrable singularities indicating that classical representation in this case is problematic. This is also confirmed by analysis of the Shrödinger equation in classical representation for the  $m \rightarrow +\infty$  case.

Further developments of the theory should address the general 1D potentials (beyond the symmetrical case) and extensions towards the multidimensional systems.

## Acknowledgments

This work was supported by Serbia-JINR collaboration program.

## Appendix A

Here we derive results presented in expressions (24).

The result for  $m = 1$  follows if we substitute  $\varepsilon = 0$  in (21) and use for  $\rho_n(x)$  the expression (5). Then we employ the relations

$$H'_n(x) = 2nH_{n-1}(x), \quad H_n(x) = 2xH_{n-1}(x) - 2(n-1)H_{n-2}(x) \quad (\text{A.1})$$

to reduce (21) to  $f_n(0) = -f_{n-1}(0)$  and since by direct calculation  $f_0(0) = 1$  the result (24),  $f_n(0) = (-1)^n$  follows.

In order to study the singular behavior of the Abel transform (21) in the limit  $\varepsilon \rightarrow 0$  and for  $m > 1$  we start from

$$\begin{aligned}\varphi_n(\varepsilon) &= \frac{f_n(\varepsilon)}{T(\varepsilon)} = -\frac{1}{\pi} \int_{\varepsilon}^{+\infty} \frac{d\rho_n(x(v))}{dv} \frac{dv}{\sqrt{v-\varepsilon}} \\ &= -\frac{1}{\pi} \int_{\varepsilon}^{\delta} \frac{d\rho_n(x(v))}{dv} \frac{dv}{\sqrt{v-\varepsilon}} - \frac{1}{\pi} \int_{\delta}^{+\infty} \frac{d\rho_n(x(v))}{dv} \frac{dv}{\sqrt{v-\varepsilon}} \\ &= -\frac{1}{\pi} \int_{\varepsilon^{\frac{1}{2m}}}^{\delta^{\frac{1}{2m}}} \frac{d\rho_n(x)}{dx} \frac{dx}{\sqrt{x^{2m}-\varepsilon}} + O(1)\end{aligned}\quad (\text{A.2})$$

We chose  $\delta$  such that  $\varepsilon^{\frac{1}{2m}} < x < \delta^{\frac{1}{2m}} \ll 1$ , and use power expansion

$$\frac{d\rho_n(x)}{dx} = \sum_{p=1}^{p_{\max}} c_{np} x^{2p-1}, \quad c_{np} = \frac{1}{(2p-1)!} \frac{d^{2p} \rho_n(x)}{dx^{2p}} \Big|_{x=0}, \quad (\text{A.3})$$

because from (3) it follows that

$$\frac{d^{2p-1} \rho_n(x)}{dx^{2p-1}} \Big|_{x=0} = 0. \quad (\text{A.4})$$

The upper limit of summation  $p_{\max}$  will be determined below. We also substitute in (A.2) the expansion

$$\frac{1}{\sqrt{x^{2m}-\varepsilon}} = \frac{1}{x^m \sqrt{1-\frac{\varepsilon}{x^{2m}}}} = \frac{1}{x^m} \sum_{k=0}^{\infty} \frac{(2k-1)!! \varepsilon^k}{(2k)!! x^{2mk}} \quad (\text{A.5})$$

with convention  $(-1)!! = 0!! = 1$ . Therefore

$$\varphi_n(\varepsilon) \approx -\frac{1}{\pi} \sum_{p=1}^{p_{\max}} c_{np} \sum_{k=0}^{\infty} \frac{(2k-1)!! \varepsilon^k}{(2k)!!} \int_{\varepsilon^{\frac{1}{2m}}}^{\delta^{\frac{1}{2m}}} x^{2p-1-m-2mk} dx + O(1). \quad (\text{A.6})$$

For  $m > 2$  we find

$$\varphi_n(\varepsilon) \approx -\frac{1}{\pi} \sum_{p=1}^{p_{\max}} c_{np} S_{mp} \varepsilon^{-\frac{1}{2} + \frac{p}{m}} + O(1), \quad (\text{A.7})$$

where

$$S_{mp} = \sum_{k=0}^{\infty} \frac{(2k-1)!!}{(2k)!! [(2k+1)m-2p]} \quad (\text{A.8})$$

is according to *Raabe's convergence criterion* [16] a convergent series.

The derivation of (A.7) is valid under the assumption that  $\varphi_n(\varepsilon)$  is a *singular function* at  $\varepsilon = 0$ , which puts the restriction on the exponent in (A.7):  $-\frac{1}{2} + \frac{p}{m} < 0$ .

This sets the upper limits in summations:

$$p_{\max} = \begin{cases} \frac{m}{2} - 1, & m - \text{even} \\ \frac{m-1}{2}, & m - \text{odd.} \end{cases} \quad (\text{A.9})$$

For  $m = 2$  we have a special case because the integral in (A.6) for  $p = 1$  and  $k = 0$  is the only one that gives singular (logarithmic) term and we find

$$\varphi_n(\varepsilon) \approx -\frac{1}{\pi} c_{n1} \log(\varepsilon^{-\frac{1}{4}}) + O(1). \quad (\text{A.10})$$

The corresponding behavior of energy distributions follows from relation  $f_n(\varepsilon) = T(\varepsilon)\varphi_n(\varepsilon)$  with  $T(\varepsilon)$  taken from (14). For  $m > 2$  we find

$$f_n(\varepsilon) \approx -\frac{1}{m\pi} B \left( \frac{1}{2m}, \frac{1}{2} \right) \sum_{p=1}^{p_{\max}} c_{np} S_{mp} \varepsilon^{-1+\frac{2p+1}{2m}}, \quad (\text{A.11})$$

and for  $m = 2$

$$f_n(\varepsilon) \approx -\frac{1}{2\pi} c_{n1} B \left( \frac{1}{4}, \frac{1}{2} \right) \varepsilon^{-\frac{1}{4}} \log(\varepsilon^{-\frac{1}{4}}). \quad (\text{A.12})$$

We note that by using (3), all coefficients in the expansion (A.3) can be calculated analytically:

$$c_{np} = \frac{(-4\varepsilon_n)^{p-1}}{(2p-1)!} c_{n1}, \quad (\text{A.13})$$

$$c_{n1} = \frac{d^2 \rho_n(x)}{dx^2} \Big|_{x=0} = \begin{cases} -2\varepsilon_n \rho_n(0), & n - \text{even} \\ 2 \left( \frac{d\psi_n}{dx} \Big|_{x=0} \right)^2, & n - \text{odd.} \end{cases} \quad (\text{A.14})$$

The relation (A.13) is valid for  $1 \leq p \leq m$  and from (A.9) we see that  $p_{\max} < m$ .

The expressions (24) and (34) in the main text are obtained by keeping only the first terms ( $p = 1$ ) in the sums (A.11) and (A.7) and the property  $c_{n1} = (-1)^{n+1} | c_{n1} |$  which follows from (A.14).

## References

- [1] N.P. Landsman, Between Classical and Quantum, in Philosophy of Science. Philosophy of Physics, eds. J. Butterfield, J. Earman, pp. 417-553, Elsevier (2007)
- [2] E.A. Solov'ev, A classical representation for the one-dimensional Schrödinger equation, Sov.Phys.-JETP **76**, 934-939 (1993)

- [3] E.A. Solov'ev, The Foundations of Quantum Physics: New Interpretation and Systematic Application, Lambert Academic Publishing, Saarbrucken (2017)
- [4] E.A. Solov'ev, Solvable problems in classical representation, Quantum Stud.: Math. Found. **6**, 161-168 (2019)
- [5] T.P. Grozdanov, E.A. Solov'ev, Classical representation for hydrogen atom in s-states, Quantum Stud.: Math. Found. **6**, 225-233 (2019)
- [6] E.A. Solov'ev, Semiclassical approach in classical representation, Quantum Stud.: Math. Found. **7**, 1-4 (2020)
- [7] E.J. Weniger, A Convergent Renormalized Strong Coupling Perturbation Expansion for the Ground State Energy of the Quartic, Sextic, and Octic Anharmonic Oscillator, Ann. Phys. (NY) **246**, 133-165 (1996)
- [8] J.K. Krieger, M.L. Lewis, C. Rosenzweig, Use of the WKB Method for Obtaining Energy Eigenvalues, J. Chem. Phys. **47**, 2942-2945 (1977)
- [9] C.M. Bender, K. Olaussen, P.S. Wang, Numerological analysis of the WKB approximation in large order, Phys. Rev. D **16**, 1740-1748 (1977)
- [10] M. Robnik, V.G. Romanovski, Some properties of WKB series, J. Phys. A: Math. Gen. **33**, 5093-5104 (2000)
- [11] A. Mushtaq, A. Noreen, K. Olaussen, I. Øverbø, Very-high-precision solutions of a class of Schrödinger type equations , Comp. Phys. Comm. **182**, 1810-1813 (2011)
- [12] P.J. Gaudreau, R.M. Slevinsky, H. Safouhi, Computing energy eigenvalues of anharmonic oscillators using the double exponential Sinc collocation method, Ann. Phys. **360**, 520-538 (2015)
- [13] D. Brandon, N. Saad, Exact and approximate solutions to Schrödinger's equation with decatic potentials, Cent. Eur. J. Phys. **11**, 279-290 (2013)
- [14] Q. Dong, G.-H. Sun, M.A. Aoki, C.-Y. Chen, S.-H. Dong, Exact solutions of a quartic potential, Mod. Phys. Lett. A **34**, 1950208 (2019)

- [15] R. Gorenflo, S. Vessella, Abel Integral Equations. Lecture Notes in Mathematics, vol 1461, Springer, Heidelberg (1991)
- [16] I.S. Gradsteyn, I.M. Ryzhik, Table of Integrals, Series and Products, Academic Press, Amsteram (2017)